THE JOURNAL OF PHYSICAL CHEMISTRY A

Article

pubs.acs.org/JPCA

Formation of 6-Methyl-1,4-dihydronaphthalene in the Reaction of the *p*-Tolyl Radical with 1,3-Butadiene under Single-Collision Conditions

Dorian S. N. Parker,[†] Beni B. Dangi,[†] and Ralf. I. Kaiser*[,†]

[†]Department of Chemistry, University of Hawaii at Manoa, Honolulu, Hawaii 96822, United States

Adeel Jamal,[‡] Mikhail Ryazantsev,[§] and Keiji Morokuma*[,‡,∥]

[‡]Department of Chemistry and Cherry L. Emerson Center for Scientific Computation, Emory University, Atlanta, Georgia 30322, United States

[§]Biomolecular NMR Laboratory, St. Petersburg State University, Botanicheskaya 17 Staryi Peterhof, St. Petersburg, Russia, 198504

[∥]Fukui Institute for Fundamental Chemistry, Kyoto University, Sakyo, Kyoto 606-8103, Japan

Supporting Information

ABSTRACT: Crossed molecular beam reactions of *p*-tolyl (C_7H_7) plus 1,3-butadiene (C_4H_6), *p*-tolyl (C_7H_7) plus 1,3-butadiene-d_6 (C_4D_6), and *p*-tolyl-d_7 (C_7D_7) plus 1,3-butadiene (C_4H_6) were carried out under single-collision conditions at collision energies of about 55 kJ mol^{-1}. 6-Methyl-1,4-dihydronaphthalene was identified as the major reaction product formed at fractions of about 94% with the monocyclic isomer (*trans*-1-*p*-tolyl-1,3-butadiene) contributing only about 6%. The reaction is initiated by *barrierless* addition of the *p*-tolyl radical to the terminal carbon atom of the 1,3-butadiene via a van der Waals complex.

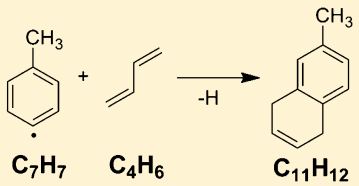

The collision complex isomerizes via cyclization to a bicyclic intermediate, which then ejects a hydrogen atom from the bridging carbon to form 6-methyl-1,4-dihydronaphthalene through a tight exit transition state located about 27 kJ mol^{-1} above the separated products. This is the dominant channel under the present experimental conditions. Alternatively, the collision complex can also undergo hydrogen ejection to form *trans*-1-*p*-tolyl-1,3-butadiene; this is a minor contributor to the present experiment. The de facto barrierless formation of a methyl-substituted aromatic hydrocarbons by dehydrogenation via a single event represents an important step in the formation of polycyclic aromatic hydrocarbons (PAHs) and their partially hydrogenated analogues in combustion flames and the interstellar medium.

1. INTRODUCTION

Polycyclic aromatic hydrocarbons (PAHs) are carcinogenic[1] and mutagenic[2] and produced by incomplete combustion of fossil fuels.[3−7] The mass growth process via cyclization of acyclic hydrocarbons to aromatic rings is thermodynamically driven by low or absent reaction barriers together with significant reaction exoergicities.[8−10] This chemistry is applicable to carbon-rich circumstellar envelopes like IRC-10216 as well,[11−14] where PAHs have been inferred to account for up to 10% of the circumstellar matter. PAHs are also thought to play an important role in the formation of prebiotic molecules,[10,15] especially with incorporation of nitrogen atoms.[16] The formation mechanisms to PAHs have been studied comprehensively within the combustion field, and theories such as the hydrogen addition acetylene addition (HACA),[17−19] ethynyl addition (EA),[20] and phenyl addition cyclization (PAC)[21,22] predict facile routes to PAHs. Interestingly, the mechanisms to alkyl-substituted PAHs have not received the same level of scrutiny as unsubstituted PAHs, while they appear to be produced in equal or greater proportions in combustion environments, particularly diesel fuel, and are also equally toxic.[23] Furthermore, the broad 3.4 μm (2491 cm^{-1}) feature[24−27] found in the unidentified infrared emission (UIE) bands is well explained by aliphatic side groups such as methyl groups over purely aromatic molecules. Finally, methyl-substituted PAHs such as methylnaphthalene and methylphenanthrene have been identified in carbonaceous chondrites, thus proposing extraterrestrial origins.[28−30]

Methyl addition reactions to closed shell PAHs possess reaction energy barriers of about 30 kJ mol^{-1} and therefore may not be the dominant route to methyl (M)PAHs in both combustion and extraterrestrial environments.[31] Recent crossed molecular beam investigations have shown that aromatic radical (phenyl C_6H_5 and *p*-tolyl $C_6H_4CH_3$) reactions with C4 hydrocarbons vinylacetylene (C_4H_4) and 1,3-butadiene (C_4H_6) form (1) naphthalene,[10] (2) 1,4-dihydronaphthalene,[32] and (3) 2-methylnaphthalene[33] without entrance barriers (Scheme 1). In this work, we build on the growing body of evidence that MPAHs can be formed by facile single-collision events through reactions of substituted aromatic radicals with

Received: October 2, 2014
Revised: November 18, 2014
Published: November 19, 2014

Scheme 1. Barrierless and Exoergic Reactions of Phenyl-Type Radicals with C4 Hydrocarbons Vinylacetylene and 1,3-Butadiene Yielding Naphthalene, 1,4-Dihydronaphthalene, and 2-Methylnaphthalene

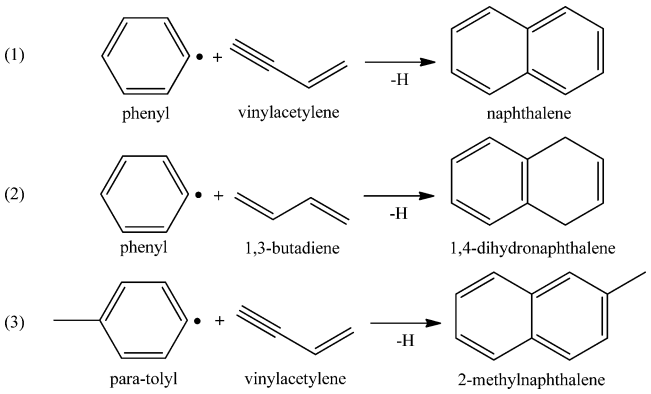

C4 hydrocarbons.[33] We present a route to form methyl-substituted 1,4-dihydronaphthalene via reaction of the *p*-tolyl radical (C_7H_7; $C_6H_4CH_3$) with 1,3-butadiene (C_4H_6).

2. EXPERIMENTAL METHOD AND ANALYSIS

Using the universal crossed molecular beams machine at the University of Hawaii, reactions of *p*-tolyl radicals ($C_6H_4CH_3$; X^2A_1) and *p*-tolyl-d_7 radical ($C_6D_4CD_3$; X^2A_1) with 1,3-butadiene (C_4H_6, X^1A_g) and deuterated 1,3-butadiene-d_6 (C_4D_6, X^1A_g) were investigated under single-collision conditions.[34] Supersonic molecular beams of the *p*-tolyl radicals were generated in the primary source chamber by single-photon photolysis of the precursor *p*-chlorotoluene (C_7H_7Cl, 98%, Aldrich; C_7D_7Cl, 98%; Bochum group) seeded in helium (99.9999%; Gaspro) at fractions of 0.2%.[33] The gas mixture was produced by bubbling the helium carrier gas at a pressure of 1300 Torr through liquid *p*-chlorotoluene in a bubbler at room temperature. It should be noted that, under our experimental conditions, using 193 nm output of an excimer at about 12 mJ, the isomerization barrier to *m*- and *o*-tolyl of 260 kJ mol^{-1} was unsurmountable.[35] The molecular beam of the helium-seeded precursor was released into the primary reaction chamber by a Proch−Trickl pulsed valve operated at 120 Hz and photolyzed 1 mm downstream of the nozzle. The radicals entrained in the molecular beam entered the reaction chamber through a 1 mm diameter skimmer, and a portion of the gas pulse was selected by a four-slit chopper wheel at 1872 μs after the pulsed valve opened. The peak intensity of the gas pulse was selected which had a peak velocity of typically 1622 ± 21 ms^{-1} and speed ratio of 8.0 ± 1.6. Table 1 refers to the full list of molecular beam characteristics for each experiment conducted. In the interaction region the radical beam was bisected at 90° by a pulsed molecular beam of neat 1,3-butadiene (Table 1) released by a second pulsed valve with a backing pressure of 550 Torr and triggered 50 μs prior to the primary pulsed valve. The products were monitored using a triply differentially pumped quadrupole mass spectrometer in time-of-flight (TOF) mode after electron-impact ionization of the neutral species with an electron energy of 80 eV. TOF spectra of the reactively scatted products were recorded over the full angular range in the plane defined by the primary and secondary reactant beams. Integration and normalization of the TOF spectra provided the product angular distribution in the laboratory frame. Information on the reaction dynamics was obtained by transformation of the experimental data into the center-of-mass (CM) frame through a forward-convolution routine.[36,37] Here, the main parameters of the forward-convolution routine are the angular flux distribution, $T(\theta)$, and the translational energy flux distribution, $P(E_T)$, in the center-of-mass system, which are adjusted to fit the experimental data, TOF spectra, and the laboratory angular distributions. The angular flux distribution, $T(\theta)$, and the translational energy flux distribution, $P(E_T)$, provide information on the reaction dynamics and reaction energy.

Table 1. Molecular Beam Characteristics: Peak Velocity (v_p (ms^{-1})), Speed Ratio (S), Collision Energy, E_{col} (kJ mol^{-1}), and Center-of-Mass Angle Θ_{CM}

	v_p (ms^{-1})	S	E_{col} (kJ mol^{-1})	Θ_{CM}
1,3-butadiene	720 ± 20	5.0 ± 1.5		
p-tolyl	1622 ± 21	8.0 ± 1.6	52.6 ± 3.6	14.2 ± 1.2
1,3-butadiene-d_6	740 ± 20	8.0 ± 1.4		
p-tolyl	1622 ± 21	8.0 ± 1.6	55.5 ± 3.5	16.7 ± 1.2
1,3-butadiene	770 ± 20	7.0 ± 1.3		
p-tolyl-d_7	1612 ± 8	7.7 ± 1.2	52.4 ± 3.6	14.7 ± 1.2

3. COMPUTATIONAL METHODS

Optimized geometries, vibrational frequencies, and zero-point vibrational energy (ZPE) were obtained using the hybrid density functional M06-2X[38,39] with the correlation-consistent cc-pVTZ basis set[40,41] calculations. Then, these optimized coordinates of all reactants, intermediates, transition states, and products were used in single-point coupled cluster CCSD(T)-F12 calculations[42−44] with the cc-pVDZ basis set. We expect that our E(CCSD(T)-F12/cc-pvdz//M06-2x/cc-pvtz+ZPE-(M06-2*x*/6-cc-pvtz)) energies should be in the chemical accuracy range of 0−8 kJ mol^{-1}. Optimized Cartesian coordinates are given in Table S1, Supporting Information. The GAUSSIAN 09[45] and MOLPRO 2012[46] programs were employed for the calculations.

Rate constants of individual reaction steps were computed using the RRKM theory[47−49] Rate constant $k(E)$ at an internal energy E for a unimolecular reaction A* → A$^{\#}$ → P can be expressed as

$$k(E) = \frac{\sigma}{h}\frac{W^{\#}(E - E^{\#})}{\rho(E)}$$

where σ is the reaction path degeneracy, h is Plank's constant, $W^{\#}(E - E^{\#})$ denotes the total number of states for the transition state (activated complex) A$^{\#}$ with a barrier $E^{\#}$, $\rho(E)$ represents the density of states at the internal energy E of the energized reactant molecule A*, and P is the product or products. The internal energy was taken as the collision energy, assuming that all of the collision energy is converted to internal vibrational energy. The harmonic approximation was employed to calculate the total number and density of states. Product branching ratios were calculated by solving first-order kinetic equations for unimolecular reactions according to the kinetics schemes devised from the ab initio potential energy diagrams.

4. EXPERIMENTAL RESULTS

To investigate the reaction dynamics of the reaction of *p*-tolyl radicals with 1,3-butadiene, three systems were studied: *p*-tolyl (C_7H_7) plus 1,3-butadiene (C_4H_6), *p*-tolyl (C_7H_7) plus 1,3-

dx.doi.org/10.1021/jp509990u | J. Phys. Chem. A 2014, 118, 12111−12119

butadiene-d_6 (C_4D_6), and *p*-tolyl-d_7 (C_7D_7) plus 1,3-butadiene (C_4H_6). In the reaction of *p*-tolyl (C_7H_7; 91 u) with 1,3-butadiene (C_4H_6; 54 u), reactive scattering signal was observed at a mass-to-charge ratio (m/z) of 144 u ($C_{11}H_{12}^+$), indicating the reaction proceeds through hydrogen atom ejection via a *p*-tolyl radical versus a hydrogen atom exchange mechanism. No adduct was observed at 145 u ($C_{11}H_{13}^+$); the signal observed could be accounted for by $^{13}CC_{10}H_{12}^+$ formed at levels of about 12%. To corroborate whether hydrogen ejection occurs from the *p*-tolyl radical and/or from the 1,3-butadiene molecule, the reaction was repeated by replacing each reactant individually by a perdeuterated sample and monitoring products associated with a hydrogen atom ejection. In the reaction of the *p*-tolyl radical with 1,3-butadiene-d_6 (C_4D_6; 60 u) a strong reactive scattering signal at m/z 150 ($C_{11}H_6D_6^+$) was observed indicating a dominant reaction channel involving hydrogen atom ejection from the *p*-tolyl reactant. For completeness, reaction of deuterated *p*-tolyl-d_7 radical (C_7D_7; 98 u) with 1,3-butadiene was investigated. A weak reactive scattering signal at m/z 151 ($C_{11}H_5D_7^+$) with intensity at a level of only 5% was observed, indicating a second reaction channel is open involving hydrogen atom ejection from the 1,3-butadiene reactant. It should be noted that scattering products for all three reactions were also observed at product masses lower by 1 and 2 u compared to the reactive scattering signal of the parent; these TOFs were superimposable after scaling with the TOFs recorded at $C_{11}H_{12}^+$, $C_{11}H_5D_7^+$, and $C_{11}H_6D_6^+$ and are therefore assigned to dissociative electron impact ionization of the products in the ionizer. In the C_7H_7 plus C_4H_6 reaction these were 143 ($C_{11}H_{11}^+$) and 142 u ($C_{11}H_{10}^+$) originating from the reactive scattering signal at 144 u ($C_{11}H_{12}^+$). For reaction of *p*-tolyl (C_7H_7) plus 1,3-butadiene-d_6 (C_4D_6) signals at 149 ($C_{11}H_5D_6^+/C_{11}H_7D_5^+$) and 148 u ($C_{11}H_4D_6^+/C_{11}H_6D_5^+$) originate from the reactive scattering product at 150 u ($C_{11}H_6D_6^+$); in the *p*-tolyl-d_7 (C_7D_7) plus 1,3-butadiene (C_4H_6) system, signals at 150 ($C_{11}H_4D_7^+/C_{11}H_6D_6^+$) and 149 u ($C_{11}H_3D_7^+/C_{11}H_5D_6^+$) originate from the reactive scattering product at 151 u ($C_{11}H_5D_7^+$).

Figures 1, 2, and 3 depict selected time-of-flight (TOF) spectra recorded at m/z 144 ($C_{11}H_{12}^+$), 150 ($C_{11}H_6D_6^+$), and 151 ($C_{11}H_5D_7^+$), respectively. The fully hydrogenated system *p*-tolyl plus 1,3-butadiene shown in Figure 1 was effectively fit with a single channel. However, the deuterated systems, *p*-tolyl plus 1,3-butadiene-d_6 and *p*-tolyl-d_7 plus 1,3-butadiene, had to be fit with two channels consisting of a nonreactive (fast) and reactive (slow) scattering signal. The reactive scattering signals shown in Figures 1, 2, and 3 represent synthesis of a product with molecular formula $C_{11}H_{12}$, $C_{11}H_6D_6$, and $C_{11}H_5D_7$, respectively, formed by reaction of the *p*-tolyl radical with 1,3-butadiene and ejection of a hydrogen atom. The laboratory angular distributions for each reaction are shown in Figures 4, 5, and 6, respectively. The red line in each system denotes the reactive scattering portion of the signal and is symmetric around the center-of-mass angles of 14.2 ± 1.2°, 16.7 ± 1.2°, and 16.7 ± 1.2°, respectively, indicative of indirect scattering dynamics via complex formation ($C_{11}H_{13}/C_{11}H_7D_6/C_{11}H_6D_7$). The nonreactive scattering portion of the signal is shown as the blue lines in the TOF and laboratory angular distributions for the *p*-tolyl plus 1,3-butadiene-d_6 and *p*-tolyl-d_7 plus 1,3-butadiene reactions shown in Figures 2, 5, 3, and 6, respectively. The nonreactive signal is most likely caused by the impurities in the primary source starting material that have a mass or fragment mass of m/z 150 and 151, respectively. To check the impact of the impurities, we replaced the secondary beam by neat argon and found a steady decay in intensity of masses at m/z 150 and 151 with increasing angle from 0° to 20°, confirming them as nonreactively scattered impurities originating from the primary beam.

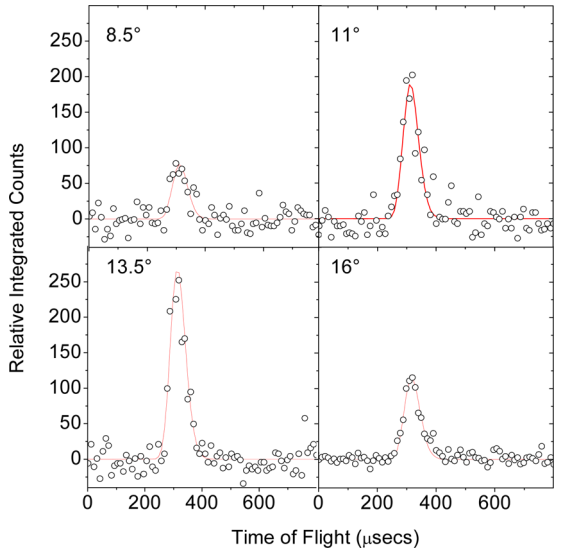

Figure 1. Time-of-flight data at various angles recorded at m/z 144 for reaction of *p*-tolyl (C_7H_7) with 1,3-butadiene (C_4H_6; $X\ ^1A_g$) at a collision energy of 52.6 ± 3.6 kJ mol^{-1}. Circles indicate the experimental data, and solid line indicates the calculated fit.

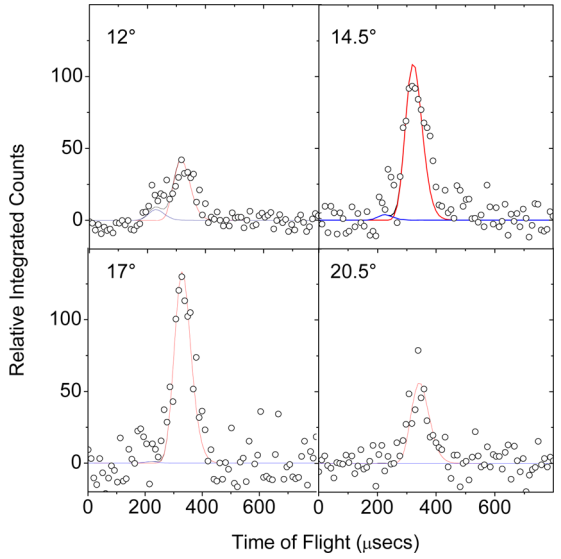

Figure 2. Time-of-flight data at various angles recorded at m/z 150 for reaction of *p*-tolyl (C_7H_7) with 1,3-butadiene-d_6 (C_4D_6; $X\ ^1A_g$) at a collision energy of 55.5 ± 3.5 kJ mol^{-1}. Circles indicate the experimental data, and solid line indicates the calculated fit.

Having established that the products formed have the molecular formula $C_{11}H_{12}$ (144 u), $C_{11}H_6D_6$ (150 u), and $C_{11}H_5D_7$ (151 u), we attempt now to elucidate the underlying reaction dynamics by converting the laboratory data to the center-of-mass frame. The center-of-mass translational energy ($P(E_T)$) and angular ($T(\theta)$) distribution fits derived from the experimental laboratory domain data are shown in Figures 7−9. Fundamentally, the center-of-mass functions in both the fully hydrogenated *p*-tolyl plus 1,3-butadiene and *p*-tolyl plus 1,3-butadiene-d_6 reactions show distinct similarities. Here, the

dx.doi.org/10.1021/jp509990u | J. Phys. Chem. A 2014, 118, 12111−12119

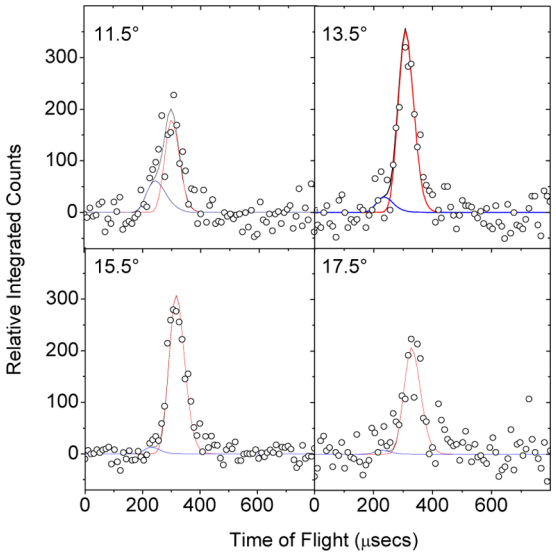

Figure 3. Time-of-flight data at various angles recorded at m/z 151 for reaction of p-tolyl-d_7 (C_7D_7) with 1,3-butadiene (C_4H_6; $X\ ^1A_g$) at a collision energy of 52.4 ± 3.6 kJ mol^{-1}. Circles indicate the experimental data, and solid line indicates the calculated fit.

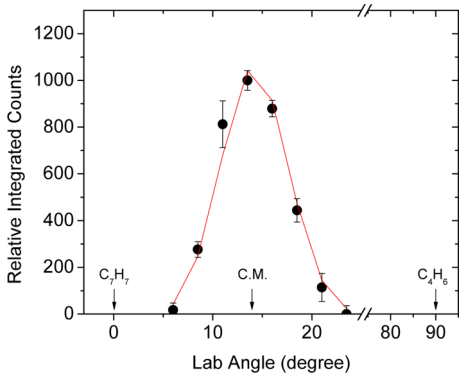

Figure 4. Laboratory angular distribution (LAB) of the $C_{11}H_{12}$ isomer(s), m/z 144, formed in the reaction of p-tolyl (C_7H_7) with 1,3-butadiene (C_4H_6; $X\ ^1A_g$) at a collision energy of 52.6 ± 3.6 kJ mol^{-1}. Circles and error bars indicate experimental data, and solid line indicates the calculated distribution.

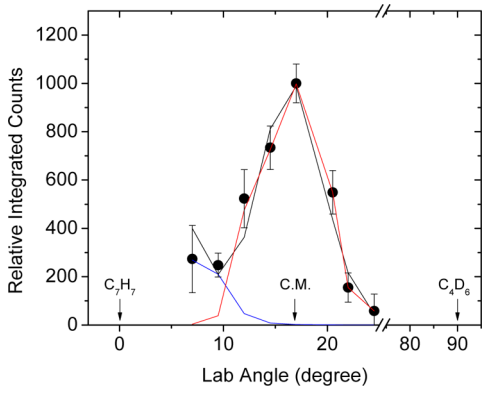

Figure 5. Laboratory angular distribution (LAB) of the $C_{11}H_6D_6$ isomer(s), m/z 150, formed in the reaction of p-tolyl (C_7H_7) with 1,3-butadiene (C_4D_6; X^1A_g) at a collision energy of 55.5 ± 3.5 kJ mol^{-1}. Circles and error bars indicate experimental data, and solid line indicates the calculated distribution.

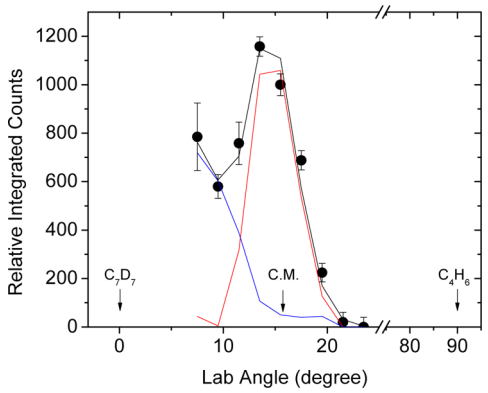

Figure 6. Laboratory angular distribution (LAB) of the $C_{11}H_5D_7$ isomer(s), m/z 151, formed in the reaction of p-tolyl (C_7D_7) with 1,3-butadiene (C_4H_6; X^1A_g) at a collision energy of 52.4 ± 3.6 kJ mol^{-1}. Circles and error bars indicate experimental data, and solid line indicates the calculated distribution.

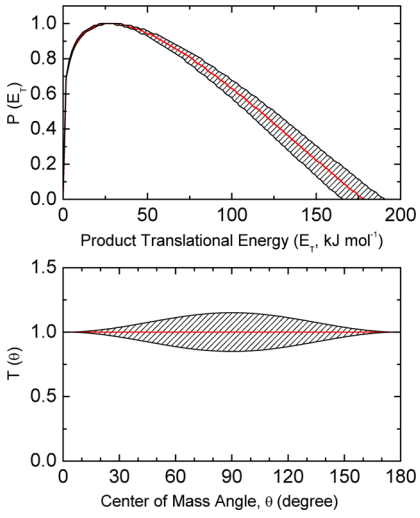

Figure 7. Center-of-mass translational energy distribution (top) and center-of-mass angular distribution (bottom) for reaction of p-tolyl (C_7H_7) with 1,3-butadiene (C_4H_6; $X\ ^1A_g$) to form $C_{11}H_{12}$ and atomic hydrogen at a collision energy of 52.6 ± 3.6 kJ mol^{-1}.

translational energy distribution depicts a maximum translational energy release of 177 ± 20 and 171 ± 20 kJ mol^{-1}, respectively. By subtracting the collision energies of 52.6 ± 3.6 and 55.5 ± 3.5 kJ mol^{-1}, we obtain reaction exoergicities of 124 ± 30 and 115 ± 30 kJ mol^{-1} in forming $C_{11}H_{12}$ and $C_{11}H_6D_6$ isomers plus atomic hydrogen for those products formed without internal excitation. The p-tolyl plus 1,3-butadiene and p-tolyl plus 1,3-butadiene-d_6 reactions center-of-mass translational energy distributions $P(E_T)$ peak at slightly different energies of about 25−35 and 15−20 kJ mol^{-1}, respectively. Peaking away from zero translational energy suggests the existence of an exit barrier and a tight exit transition state to product formation,[50] which is indicative of repulsive carbon−hydrogen bond ruptures involving a significant electron rearrangement in forming the final products from the reaction intermediates. The average amount of energy released into the translational degrees of freedom of the products are 66 ± 20 (37 ± 6%) and 53 ± 20 kJ mol^{-1} (31 ± 6%) of the total available energy, respectively, indicating that at least one reaction channel to form the $C_{11}H_{12}/C_{11}H_6D_6$ isomer(s) plus atomic hydrogen has a tight exit transition state and therefore

dx.doi.org/10.1021/jp509990u | J. Phys. Chem. A 2014, 118, 12111−12119

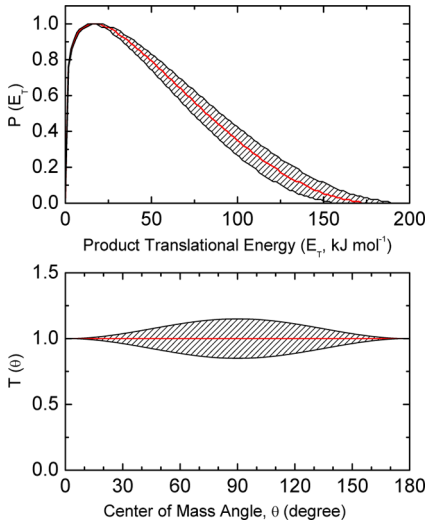

Figure 8. Center-of-mass translational energy distribution (top) and center-of-mass angular distribution (bottom) for reaction of *p*-tolyl (C_7H_7) with 1,3-butadiene-d_6 (C_4D_6; $X\ ^1A_g$) to form $C_{11}H_6D_6$ and atomic hydrogen at a collision energy of 55.5 ± 3.5 kJ mol^{-1}.

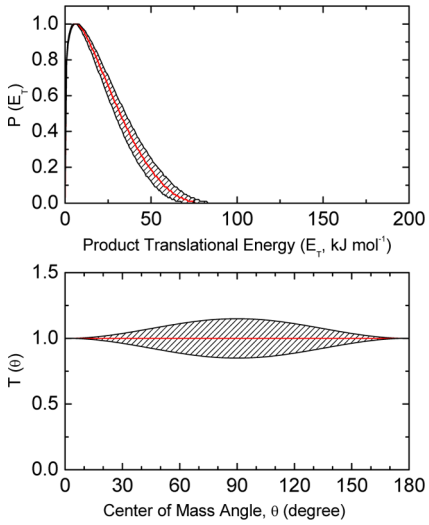

Figure 9. Center-of-mass translational energy distribution (top) and center-of-mass angular distribution (bottom) for reaction of *p*-tolyl-d_7 (C_7D_7) with 1,3-butadiene (C_4H_6; $X\ ^1A_g$) to form $C_{11}H_5D_7$ and atomic hydrogen at a collision energy of 52.4 ± 3.6 kJ mol^{-1}.

suggests repulsive carbon−hydrogen bond rupture. Conversely, the *p*-tolyl-d_7 plus 1,3-butadiene reaction shows a markedly different maximum translational energy release of the translational energy distribution of only 75 kJ mol^{-1}, which after subtraction of the collision energy of 52.4 ± 3.6 kJ mol^{-1} gives a low reaction energy of 22 ± 30 kJ mol^{-1} in forming the product $C_{11}H_5D_7$ isomers plus atomic hydrogen. Here, peaking of the translational energy distribution occurs close to zero translational energy at about 5 kJ mol^{-1}, which is indicative of a rather loose exit transition state.

The center-of-mass angular distributions, $T(\theta)$, shown in the bottom of Figures 7−9 are identical for all three systems and show intensity over the full angular range, indicating indirect complex forming reaction mechanisms forming $C_{11}H_{13}$/$C_{11}H_7D_6$/$C_{11}H_6D_7$ intermediates.[50] Best fits yield isotropic (flat), forward−backward distributions, indicating that the lifetime of the decomposing complex is longer than its rotational period.[50] The isotropy of the center-of-mass angular distributions, $T(\theta)$, is indicative of a weakly polarized system in which the initial orbital angular momentum does not couple well with the final orbital angular momentum due to the light mass of the departing hydrogen atom. Considering angular momentum conservation, the initial angular momentum is channeled preferentially into the rotational degrees of freedom of the $C_{11}H_{12}$/$C_{11}H_6D_6$/$C_{11}H_5D_7$ product(s). In summary, we consider that within the error boundaries of the experiments, both the *p*-tolyl plus 1,3-butadiene and *p*-tolyl plus 1,3-butadiene-d_6 reactions display the same reaction dynamics and therefore represent the same reaction channel(s), while the *p*-tolyl plus 1,3-butadiene-d_6 reaction displays markedly different reaction dynamics and therefore possibly distinct reaction products and dynamics.

5. THEORETICAL RESULTS

The mechanisms and products formed in the reaction of *p*-tolyl radical (C_7H_7; $X\ ^2A_1$) with 1,3-butadiene ($X\ ^1A'$) are also predicted based on ab initio calculations of the $C_{11}H_{13}$ potential energy surface (PES). It should be noted here that use of deuterated reactants alters vibrational and rotational energies and changes the effective barriers and exoergicities from those of fully hydrogenated systems by only 5 kJ mol^{-1} on average and never more than 10 kJ mol^{-1}; these values were previously recognized in reactions leading to indene (C_9H_9/C_9D_9)[9] or 2-methylnaphthalene ($C_{11}H_{10}$/$C_{11}H_3D_7$)[33] formation in which both hydrogenated and deuterated species were calculated. The small discrepancy in calculated energies is below one-half of the experimental error of the reaction energies and therefore bares no influence on the interpretation of the data. Therefore, we used the values calculated for the fully hydrogenated $C_{11}H_{13}$ species for interpretation of the energetics in all three reactions conducted experimentally. We present figures of the potential energy surfaces with zero-point energy correction for reactions starting from *p*-tolyl (C_7H_7) plus 1,3-butadiene-d_6 (C_4D_6) in order to identify origins of hydrogen/deuterium atoms.

p-Tolyl addition can occur barrierlessly to the terminal CH_2 sp^2 carbon of 1,3-butadiene (Figure 10) or to the central CH sp^2 carbon with an entrance barrier (Figure 11). For addition to the terminal carbon atoms of 1,3-butadiene, a potential energy scan (Figure S1, Supporting Information) calculated at the M06-2x/cc-pvtz level of theory varying the C−C bond distance of the para carbon atom of *p*-tolyl with the terminal carbon atom of 1,3-butadiene along the minimum energy path shows an attractive character as the C−C bond length decreases to 2.4 Å until a van der Waals complex forms with an energy 7 kJ mol^{-1} below the reactants. A slight structural rearrangement of the van der Waals complex over a barrier of 2 kJ mol^{-1} leads to the initial intermediate **1**. Formation of a collision complex **1** through formation of a van der Waals complex below the energy of the reactants means the reaction is de facto barrierless and can occur at very low temperatures, such as about 10 K as present in cold molecular clouds.

The forward and reverse RRKM rate constants of all individual reaction steps of *p*-tolyl addition to the terminal CH_2 sp^2 carbon of 1,3-butadiene are given in Table S1, Supporting Information. Product branching ratios are calculated at the 0−60 kJ mol^{-1} collision energy in 5 kJ mol^{-1} increments and given in Table S2, Supporting Information.

5.1. Addtion of *p*-Tolyl to the Terminal Carbon of 1,3-Butadiene. Addition of *p*-tolyl to the terminal carbon of 1,3-butadiene occurs barrierlessly, leading to the initial intermediate

dx.doi.org/10.1021/jp509990u | J. Phys. Chem. A 2014, 118, 12111−12119

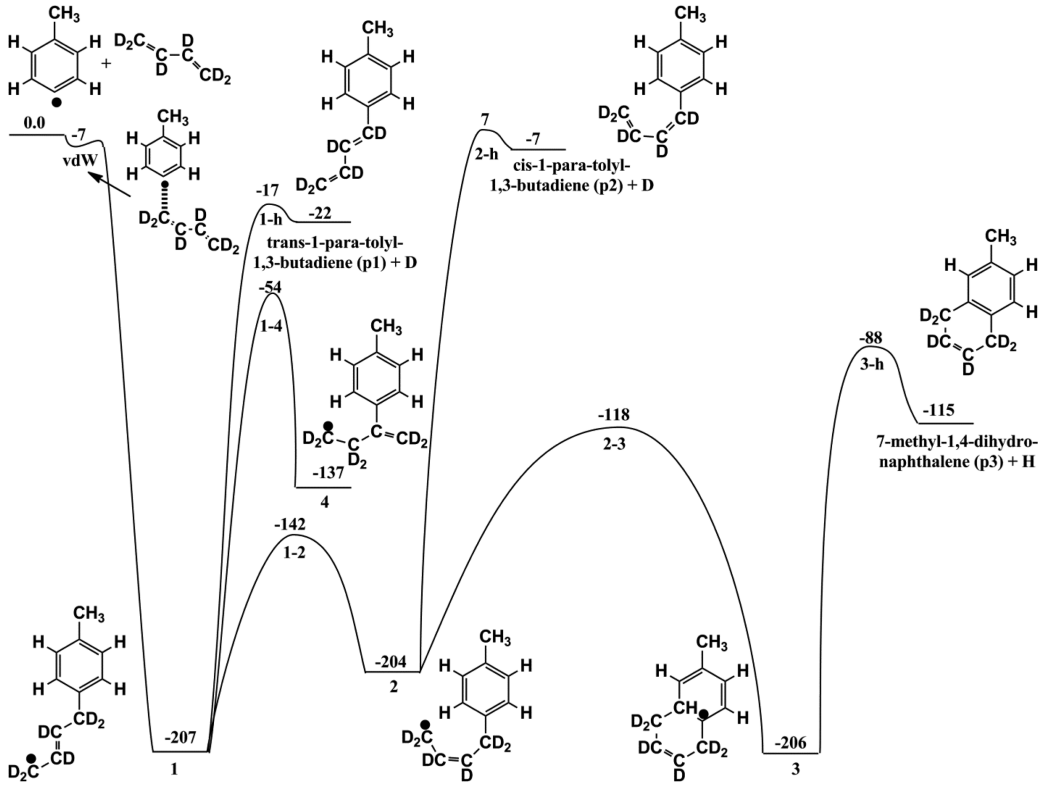

Figure 10. Potential energy diagram for terminal addition of *p*-tolyl to 1,3-butadiene-d_6. Energies for intermediates, transition states, and products are given relative to the reactants energy (in kJ mol^{-1}) at the E(CCSD(T)-F12/cc-pvdz//M06-2x/cc-pvtz+ZPE(M06-2*x*/6-cc-pvtz)) level of theory.

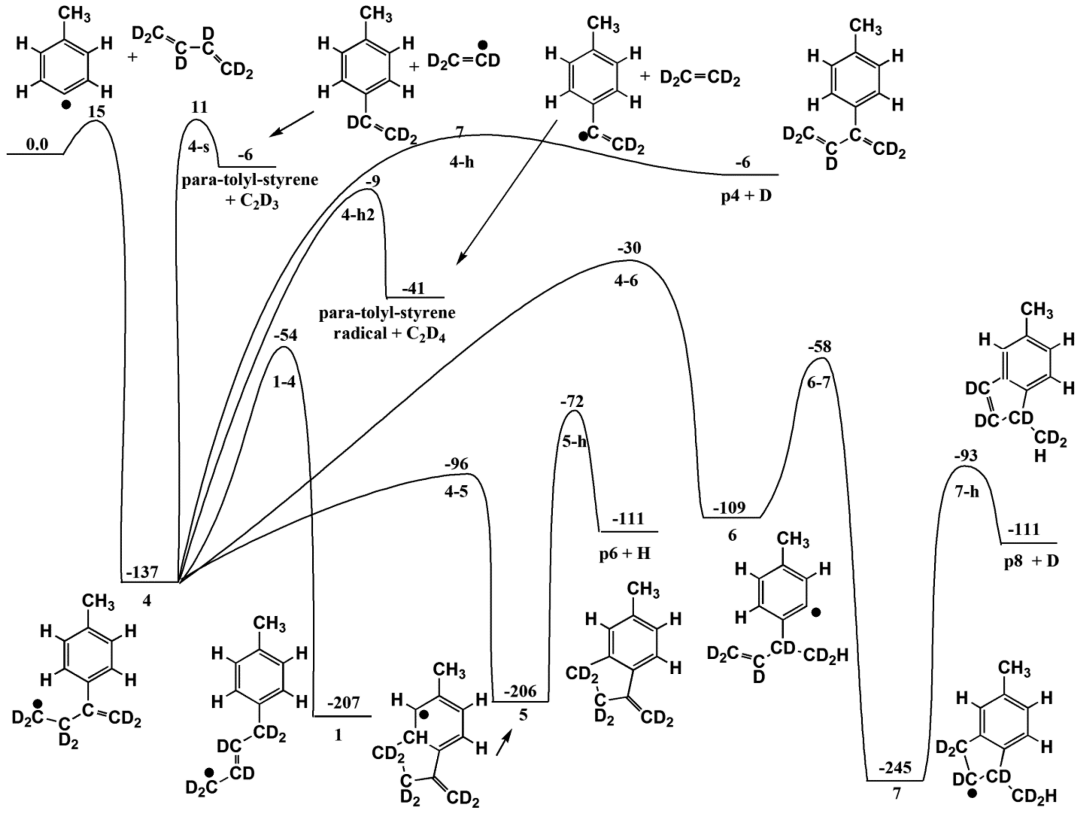

Figure 11. Potential energy diagram for central addition of *p*-tolyl to 1,3-butadiene-d_6. Energies for intermediates, transition states, and products are given relative to the reactants energy (in kJ mol^{-1}) at the E(CCSD(T)-F12/cc-pvdz//M06-2x/cc-pvtz+ZPE(M06-2*x*/6-cc-pvtz)) level of theory.

1 stabilized by 207 kJ mol^{-1} with respect to the separated reactants. Then **1** can eject a deuterium atom to form *trans*-1-*p*-tolyl-1,3-butadiene (**p1**) with an exoergicity of 22 kJ mol^{-1} and a loose exit transition state with a reverse barrier of only 5 kJ

dx.doi.org/10.1021/jp509990u | J. Phys. Chem. A 2014, 118, 12111−12119

mol^{-1}. However, a more energetically favorable channel for **1** is a rotation around a single bond to lead to **2** through a barrier of 65 kJ mol^{-1}. Intermediate **2** can eject a deuterium atom, leading to *cis*-1-*p*-tolyl-1,3-butadiene (**p2**) with an overall exoergicity of 7 kJ mol^{-1}. Deuterium ejection is achieved through a loose exit transition state 14 kJ mol^{-1} above the products. Alternatively, **2** can cyclize forming **3** over a barrier of 86 kJ mol^{-1}. Intermediate **3** can then eject an hydrogen atom through an exit transition state residing 27 kJ mol^{-1} above the separated products, leading to the product 6-methyl-1,4-dihydronaphthalene (**p3**) with an overall exoergicity of 115 kJ mol^{-1}. From intermediate **1**, an alternative transition state exists, leading to **2**, the initial intermediate of the central carbon addition (to be discussed in the next section), via a tricarbon cyclic TS structure over a 153 kJ mol^{-1} energy barrier. Product branching ratios (Table S2, Supporting Information) show that the reaction channel leading to 6-methyl-1,4-dihydronaphthalene (**p3**) plus atomic hydrogen is the dominant product channel, with a product branching ratio of 100% at 0 kJ mol^{-1} collision energy, lowering to 93% at 60 kJ mol^{-1} collision energy. The remaining competing product forming channel is to *trans*-1-*p*-tolyl-1,3-butadiene (**p1**) plus atomic deuterium.

5.2. Addition of *p*-Tolyl to the Central Carbon of 1,3-Butadiene. Addition of *p*-tolyl to the central carbon of 1,3-butadiene has to overcome a 15 kJ mol^{-1} entrance barrier that leads to **4**. Intermediate **4** can go through three possible fragmentation or ejection channels to give different products or three isomerization channels to give alternative intermediates. Products can be formed by either deuterium ejection from the central bonding carbon of 1,3-butadiene to form **p4** plus atomic deuterium with a barrier at +7 kJ mol^{-1} above the reactants and an exoergicity of 6 kJ mol^{-1} or vinyl (C_2D_3) radical ejection by cleavage of the central C−C bond on the 1,3-butadiene fragment leading to *p*-tolyl-styrene (**p5**) with a barrier at +11 kJ mol^{-1} above the reactants and an exoergicity of 6 kJ mol^{-1}. Alternatively, **4** can eject an ethylene (C_2D_4) molecule to form *p*-tolyl-styrene radical (**p7**) through a tight exit transition state at −9 kJ mol^{-1} with an exoergicity of 41 kJ mol^{-1}. Isomerizations available for **4** can be either to the terminal addition intermediate **1** (Figure 10) over a large barrier of 83 kJ mol^{-1} via a tricyclic intermediate or to **5** over a 56 kJ mol^{-1} barrier by cyclization. The latter is followed by ejection of a hydrogen atom, leading to the dimethyl-substituted indene product **p6** with a reaction exoergicity of 111 kJ mol^{-1} through a very tight exit transition state of 61 kJ mol^{-1}. The remaining option for **4** is to undergo a 1−4 hydrogen shift over a 30 kJ mol^{-1} barrier, leading to **6** with subsequent cyclization over a barrier of 51 kJ mol^{-1}, leading to **7**. From **7** deuterium ejection over a barrier of 152 kJ mol^{-1} and through a tight exit transition state leads to the product **p8** with an exoergicity of 111 kJ mol^{-1}.

Since addition of *p*-tolyl to the central carbon of 1,3-butadiene has an entrance barrier of 15 kJ mol^{-1}, RRKM theory was not applied and the reaction is concluded to be less feasible at the present low collision energy.

We also considered deuterium atom abstractions of 1,3-butadiene from *p*-tolyl, leading to toluene and a 1,3-butadiene radical. There are two possible deuterium atom abstractions that can occur: one from the terminal carbon of 1,3-butadiene or one from the central carbon of 1,3-butadiene. As shown in Figure S2, Supporting Information, both deuterium atom abstraction channels have entrance barriers of 38 and 28 kJ mol^{-1} relative to the energy of the reactants, respectively, and can be ignored completely under the present experimental conditions. The former D-abstraction channel leads to toluene plus $\dot{C}D{=}CD{-}C{=}CD_2$ (*n*-C_4D_5) at an overall exoergicity of 3 kJ mol^{-1} relative to the energy of the reactants, while the latter leads to toluene plus $CD_2{=}\dot{C}{-}CD{=}CD_2$ (*i*-C_4D_5) at an overall exoergicity of 15 kJ mol^{-1} relative to the energy of the reactants.

6. DISCUSSION

Having presented the potential energy surfaces, we shall now interpret the experimental reaction dynamics accordingly to ascertain the actual reaction mechanism taken and products formed in the experiment. First, let us inspect the reaction products formed. Here, the experimentally determined reaction energy of the high-energy and dominant reaction channel forming $C_{11}H_{12}/C_{11}H_6D_{12}$ isomer(s) plus atomic hydrogen is about 120 ± 30 kJ mol^{-1}. This value matches well those calculated for formation of 6-methyl-1,4-dihydronaphthalene plus atomic hydrogen of 115 kJ mol^{-1} and formation of **p8** plus atomic hydrogen of 111 kJ mol^{-1}. The difference between the formation of 6-methyl-1,4-dihydronaphthalene and **p8** is that the former ejects a hydrogen atom from *p*-tolyl and the latter from 1,3-butadiene. Therefore, we can conclude the dominant reaction channel in *p*-tolyl radical plus 1,3-butadiene leads to formation of 6-methyl-1,4-dihydronaphthalene plus atomic hydrogen. The reaction is initiated by addition to the C1 carbon of 1,3-butadiene barrierlessly via a van der Waals complex to reach intermediate **1**, which isomerizes to **2** followed by cyclization to **3** and hydrogen ejection over a tight exit transition state of 27 kJ mol^{-1} to yield 6-methyl-1,4-dihydronaphthalene. It should be noted that at our collision energy of about 50 kJ mol^{-1} addition to the central carbon atom is possible by overcoming the 15 kJ mol^{-1} energy barrier to form intermediate **4** from where isomerization can lead to intermediate **1** via a tricyclic transition state. However, we anticipate this route to not be the dominant route due to the entrance barrier.

The off zero peaking of the center-of-mass translational energy distribution for both *p*-tolyl plus 1,3-butadiene and *p*-tolyl plus 1,3-butadiene-d_6 reactions of 15−35 kJ mol^{-1} is indicative of a tight exit transition state, matching well that calculated for 6-methyl-1,4-dihydronaphthalene formation. The center-of-mass angular distribution in both reactions is isotropic, not yielding any additional insight into the reaction dynamics taken in this instance. However, it should be noted that hydrogen ejection in the direction perpendicular to the plane of the molecule and parallel to the principal rotation axis could result in a preferential ejection direction and cause a peaked angular distribution. In the reaction of phenyl plus vinylacetylene[10] strong peaking was observed, while in the reaction of phenyl plus 1,3-butadiene[32] peaking was less pronounced. This suggests that as the molecule becomes more saturated less peaking in the angular distribution might be expected, resulting from a reduced rigidity of the C_4H_6 moiety compared to the C_4H_4 moiety and therefore a greater scope of angles for hydrogen ejection to occur from, blurring any preferentiality relative to the principal rotation axis. If we couple this with the fact that in the reaction of *p*-tolyl plus vinylacetylene[33] the peaking was already mild due to the influence of the methyl group we can anticipate weak if any peaking of the center-of-mass angular distribution.

In the reaction of *p*-tolyl-d_7 plus 1,3-butadiene through hydrogen atom loss we observed a low yield and low reaction

energy reaction channel. Here, the reaction energy is about 22 ± 30 kJ mol^{-1} when forming $C_{11}H_5D_7$ isomer(s) plus atomic hydrogen (Figure 9). Computations predict formation of *trans*-1-*p*-tolyl-butadiene and *p*-tolyl-propenyl-α-methylene (**p4**) with reaction exoergicities of 22 ± 8 (Figure 10) and 25 ± 8 kJ mol^{-1} (Figure 11) that are produced from hydrogen ejection from the 1,3-butadiene moiety. The reactions both proceed through a *p*-tolyl addition−hydrogen atom elimination mechanism at the C1 and C2 carbon atoms of 1,3-butadiene via intermediates **1** and **4**, respectively. Which is the dominant product? Formation of **p4** is expected to be less favorable due to the 15 kJ mol^{-1} entrance barrier necessary to add *p*-tolyl to the C2 carbon of 1,3-butadiene. The center-of-mass translational energy distribution indicates a low exit barrier of about 5 kJ mol^{-1} which is identical to that calculated for *trans*-1-*p*-tolyl-butadiene plus atomic hydrogen formation. The center-of-mass angular distribution is isotropic, indicating formation of a product without a preferential hydrogen ejection direction relative to the principal rotation axis as found in hydrogen ejection from the C1 carbon of intermediate **1**. Furthermore, RRKM theory predicts a branching ratio of only 6% of *trans*-1-*p*-tolyl-butadiene, which matches qualitatively the branching ratio between both channels.

In summary, under our experimental conditions *p*-tolyl likely adds to 1,3-butadiene at the C1 position in an overall barrierless addition via a van der Waals complex, which after isomerization leads to formation of 6-methyl-1,4-dihydronaphthalene through hydrogen atom ejection. To a minor extent the reaction undergoes hydrogen atom ejection immediately after radical addition from the C1 position of 1,3-butadiene to form the monocyclic hydrocarbon *trans*-1-*p*-tolyl-1,3-butadiene. The barrierless nature of this reaction implies that it could occur at temperatures as low as 10 K, as prevalent in cold molecular clouds. This mechanism adds to the increasing catalog of aromatic radical reactions with C_4H_x (x = 4, 6) hydrocarbons[10,32,33] (Scheme 1) that lead to facile PAH formation at low temperatures. PAH formation at low temperatures has implications for the chemistry of hydrocarbon-rich atmospheres of planets and their moons in the outer Solar System such as on Titan. It should be noted that under our experimental conditions *p*-tolyl could bind to the C2 position of 1,3-butadiene and produce a second monocyclic hydrocarbon **p4** through a radical addition−hydrogen atom elimination mechanism. Finally, it is important to address reaction pathways involving hydrogen atom abstraction from the C1 and C2 carbon atoms forming toluene and *i*-C_4H_5 and *n*-C_4H_5, respectively (Figure S2, Supporting Information). These hydrogen atom abstraction pathways have barriers of 28 and 38 kJ mol^{-1} and are exoergic by 15 and 3 kJ mol^{-1}, respectively. These high entrance barriers imply that these pathways cannot compete in cold environments like in cold molecular clouds; however, they might be open in combustion flames.

7. CONCLUSION

We conducted crossed molecular beam experiments of *p*-tolyl plus 1,3-butadiene, *p*-tolyl plus 1,3-butadiene-d_6, and *p*-tolyl-d_7 plus 1,3-butadiene at collision energies of 52.6, 55.5, and 52.4 kJ mol^{-1}. These experiments were combined with electronic structure and RRKM calculations of the $C_{11}H_{13}$ potential energy surface. Our investigations show that 6-methyl-1,4-dihydronaphthalene is formed via indirect scattering dynamics through a bimolecular collision of two non-PAH reactants: the *p*-tolyl radical and 1,3-butadiene. To a lesser extent, *trans*-1-*p*-tolyl-butadiene is also formed. This reaction is initiated by addition of the *p*-tolyl radical to the terminal (C1/C4) carbon, followed by hydrogen atom ejection or isomerization and cyclization of the doublet radical intermediates to reach the alkylated substituted-PAH. Addition at the vinyl group C1 was found to be *barrierless*, proceeding through a van der Waals complex. The barrierless route to 6-methyl-1,4-dihydronaphthalene means it can occur at ultralow temperatures of the ISM of 10 K as well as hydrocarbon-rich atmospheres of planets and their moons in the outer Solar System. Facile synthetic pathways to MPAHs in cold molecular clouds even at temperatures as low as 10 K could be the source of material responsible for the broad 3.4 μm feature in the UIEs.

■ ASSOCIATED CONTENT

Supporting Information

RRKM rate constants and statistical branching ratios from *p*-tolyl addition to the C^1 carbon atom of 1,3-butadiene; Cartesian coordinates of all optimized structures are also tabulated. This material is available free of charge via the Internet at http://pubs.acs.org.

■ AUTHOR INFORMATION

Corresponding Authors

*E-mail: ralfk@hawaii.edu.

*E-mail: keiji.morokuma@emory.edu.

Notes

The authors declare no competing financial interest.

■ ACKNOWLEDGMENTS

This work was supported by the U.S. Department of Energy, Basic Energy Sciences (DE-FG02-03ER15411) at the University of Hawaii and also by the Air Force Office of Scientific Research (FA9550-12-1-0472) at Emory University.

■ REFERENCES

(1) Baird, W. M.; Hooven, L. A.; Mahadevan, B. Carcinogenic Polycyclic Aromatic Hydrocarbon-DNA Adducts and Mechanism of Action. *Environ. Mol. Mutagen.* **2005**, *45*, 106−114.

(2) Finlayson-Pitts, B. J.; Pitts, J. N., Jr. Tropospheric Air Pollution: Ozone, Airborne Toxics, Polycyclic Aromatic Hydrocarbons, and Particles. *Science* **1997**, *276*, 1045−52.

(3) Tian, Z.; Pitz, W. J.; Fournet, R.; Glaude, P. A.; Battin-Leclerc, F. A Detailed Kinetic Modeling Study Toluene Oxidation in a Premixed Flame. *Proc. Combust. Inst.* **2011**, *33*, 233−241.

(4) Yang, B.; Li, Y.; Wei, L.; Huang, C.; Wang, J.; Tian, Z.; Yang, R.; Sheng, L.; Zhang, Y.; Qi, F. An Experimental Study of the Premixed Benzene/Oxygen/Argon Flame with Tunable Synchrotron Photoionization. *Proc. Combust. Inst.* **2007**, *31*, 555−563.

(5) Li, Y.; Zhang, L.; Tian, Z.; Yuan, T.; Wang, J.; Yang, B.; Qi, F. Experimental Study of a Fuel-Rich Premixed Toluene Flame at Low Pressure. *Energy Fuels* **2009**, *23*, 1473−1485.

(6) Huang, C.; Wei, L.; Yang, B.; Wang, J.; Li, Y.; Sheng, L.; Zhang, Y.; Qi, F. Lean Premixed Gasoline/Oxygen Flame Studied with Tuneable Synchrotron Vacuum UV Photoionization. *Energy Fuels* **2006**, *20*, 1505−1513.

(7) Olten, N.; Senkan, S. M. Formation of Polycyclic Aromatic Hydrocarbons in an Atmospheric Pressure Ethylene Diffusion Flame. *Combust. Flame* **1999**, *118*, 500−507.

(8) Kislov, V. V.; Islamova, N. I.; Kolker, A. M.; Lin, S. H.; Mebel, A. M. Hydrogen Abstraction Acetylene Addition and Diels-Alder Mechanisms of PAH Formation: A Detailed Study Using First Principles Calculations. *J. Chem. Theory Comput.* **2005**, *1*, 908−924.

(9) Parker, D. S. N.; Zhang, F.; Kaiser, R. I.; Kislov, V. V.; Mebel, A. M. Indene Formation under Single-Collision Conditions from the

Reaction of Phenyl Radicals with Allene and Methylacetylene- A Crossed Molecular Beam and Ab Initio Study. *Chem.—Asian J.* **2011**, *6*, 3035−3047.
(10) Parker, D. S. N.; Zhang, F.; Kim, Y. S.; Kaiser, R. I.; Landera, A.; Kislov, V. V.; Mebel, A. M.; Tielens, A. G. G. M. Low Temperature Formation of Naphthalene and Its Role in the Synthesis of PAHs (Polycyclic Aromatic Hydrocarbons) in the Interstellar Medium. *Proc. Natl. Acad. Sci. U.S.A.* **2012**, *109*, 53−58.
(11) Duley, W. W. Polycyclic Aromatic Hydrocarbons, Carbon Nanoparticles and the Diffuse Interstellar Bands. *Faraday Discuss.* **2006**, *133*, 415−425.
(12) Salama, F.; Galazutdinov, G. A.; Krelowski, J.; Allamandola, L. J.; Musaev, F. A. Polycyclic Aromatic Hydrocarbons and the Diffuse Interstellar Bands. A Survey. *Astrophys. J.* **1999**, *526*, 265−273.
(13) Ricks, A. M.; Douberly, G. E.; Duncan, M. A. The Infrared Spectrum of Protonated Naphthalene and Its Relevance for the Unidentified Infrared Bands. *Astrophys. J.* **2009**, *702*, 301−306.
(14) Cherchneff, I. The Formation of Polycyclic Aromatic Hydrocarbons in Evolved Circumstellar Environments. *EAS Publ. Ser.* **2011**, *46*, 177−189.
(15) Allamandola, L. J. PAHs and Astrobiology. *EAS Publ. Ser.* **2011**, *46*, 305−317.
(16) Charnley, S. B.; Kuan, Y. J.; Huang, H.-C.; Botta, O.; Butner, H. M.; Cox, N.; Despois, D.; Ehrenfreund, P.; Kisiel, Z.; Lee, Y.-Y.; Markwick, A. J.; Peeters, Z.; Rodgers, S. D. Astronomical Searches for Nitrogen Heterocycles. *Adv. Space Res.* **2005**, *36*, 137−145.
(17) Bittner, J. D.; Howard, J. B. Particulate Carbon: Formation During Combustion. *Proc. Int. Symp. Combust.* **1981**, *18*, 1105−1116.
(18) Frenklach, M.; Wang, H. Detailed Modeling of Soot Particle Nucleation and Growth. *Proc. Combust. Inst.* **1991**, *23*, 1559−1566.
(19) Parker, D. S. N.; Kaiser, R. I.; Troy, T. P.; Ahmed, M. Hydrogen Abstraction/Acetylene Addition Revealed. *Angew. Chem., Int. Ed.* **2014**, *53*, 7740−7744.
(20) Mebel, A. M.; Kislov, V. V.; Kaiser, R. I. Photoinduced Mechanism of Formation and Growth of Polycyclic Aromatic Hydrocarbons in Low-Temperature Environments Via Successive Ethynyl Radical Additions. *J. Am. Chem. Soc.* **2008**, *130*, 13618−13629.
(21) Shukla, B.; Koshi, M. Comparative Study on the Growth Mechanisms of PAHs. *Combust. Flame* **2011**, *158*, 369−375.
(22) Comandini, A.; Malewicki, T.; Brezinsky, K. Chemistry of Polycyclic Aromatic Hydrocarbons Formation from Phenyl Radical Pyrolysis and Reaction of Phenyl and Acetylene. *J. Phys. Chem. A* **2012**, *116*, 2409−2434.
(23) Liang, F.; Lu, M.; Keener, T. C.; Liu, Z.; Khang, S.-J. The Organic Composition of Diesel Particulate Matter, Diesel Fuel and Engine Oil of a Non-Road Diesel Generator. *J. Environ. Monit.* **2005**, *7*, 983−988.
(24) Kwok, S.; Zhang, Y. Mixed Aromatic−Aliphatic Organic Nanoparticles as Carriers of Unidentified Infrared Emission Features. *Nature* **2011**, *479*, 80−83.
(25) Li, A.; Draine, B. T. The Carriers of the Interstellar Unidentified Infrared Emission Features: Aromatic or Aliphatic? *Astrophys. J.* **2012**, *760*, L31−L35.
(26) Geballe, T. B.; Tielens, A. G. G. M.; Kwok, S.; Hrivnak, B. J. Unusual 3 Micron Emission Features in Three Proto-Planetary Nebulae. *Astrophys. J.* **1992**, *387*, L89−L91.
(27) Hrivnak, B. J.; Geballe, T. B.; Kwok, S. A Study of the 3.3 and 3.4 μm Emission Features in Protoplanetary Nebulae. *Astrophys. J.* **2007**, *662*, 1059−1066.
(28) Elsila, J. E.; De Leon, N. P.; Buseck, P. R.; Zare, R. N. Alkylation of Polycyclic Aromatic Hydrocarbons in Carbonaceous Chondrites. *Geochim. Cosmochim. Acta* **2005**, *69*, 1349−1357.
(29) Spencer, M. K.; Hammond, M. R.; Zare, R. N. Laser Mass Spectrometric Detection of Extraterrestrial Aromatic Molecules: Mini-Review and Examination of Pulsed Heating Effects. *Proc. Natl. Acad. Sci. U.S.A.* **2008**, *105*, 18096−18101.
(30) Sephton, M. A. Organic Compounds in Carbonaceous Meteorites. *Nat. Prod. Rep.* **2002**, *19*, 292−311.
(31) Holt, P. M.; Kerr, J. A. Kinetics of Gas-Phase Addition Reactions of Methyl Radicals. I. Addition to Ethylene, Acetylene, and Benzene. *Int. J. Chem. Kinet.* **2004**, *9*, 185−200.
(32) Kaiser, R. I.; Parker, D. S. N.; Zhang, F.; Landera, A.; Kislov, V. V.; Mebel, A. M. PAH Formation under Single Collision Conditions: Reaction of Phenyl Radical and 1,3-Butadiene to Form 1,4-Dihydronaphthalene. *J. Phys. Chem. A* **2012**, *116*, 4248−4258.
(33) Parker, D. S. N.; Dangi, B. B.; Kaiser, R. I.; Jamal, A.; Ryazantsev, M. N.; Morokuma, K.; Korte, A.; Sander, W. An Experimental and Theoretical Study on the Formation of 2-Methylnaphthalene ($C_{11}H_{10}/C_{11}H_3D_7$) in the Reactions of the *p*-Tolyl (C_7H_7) and *p*-Tolyl-d_7 (C_7D_7) with Vinylacetylene (C_4H_4). *J. Phys. Chem. A* **2014**, *118*, 2709−2718.
(34) Kaiser, R. I.; Maksyutenko, P.; Ennis, C.; Zhang, F.; Gu, X.; Krishtal, S. P.; Mebel, A. M.; Kostko, O.; Ahmed, M. Untangling the Chemical Evolution of Titan's Atmosphere and Surface-from Homogeneous to Heterogeneous Chemistry. *Faraday Discuss.* **2010**, *147*, 429−478.
(35) Dames, E.; Wang, H. Isomerization Kinetics of Benzylic and Methylphenyl Type Radicals in Single-Ring Aromatics. *Proc. Combust. Inst.* **2013**, *34*, 307−314.
(36) Vernon, M. Ph.D. Thesis, University of California, Berkeley, CA, 1981.
(37) Weiss, M. S. Ph.D. Thesis, University of California, Berkeley, CA, 1986.
(38) Zhao, Y.; Truhlar, D. *Theor. Chem. Acc.* **2008**, *120*, 215−241.
(39) Papajak, E.; Leverentz, H.; Zheng, J.; Truhlar, D. G. Efficient Diffuse Basis Sets: cc-pVxZ+ and maug-cc-pVxZ. *J. Chem. Theory Comput.* **2009**, *5*, 1197−1202.
(40) Dunning, T.; Peterson, K.; Wilson, A. Gaussian Basis Sets for Use in Correlated Molecular Calculations. X. The Atoms Aluminum through Argon Revisited. *J. Chem. Phys.* **2001**, *114*, 9244−9253.
(41) Dunning, T. H., Jr. Gaussian Basis Sets for Use in Correlated Molecular Calculations. I. The Atoms Boron through Neon and Hydrogen. *J. Chem. Phys.* **1989**, *90*, 1007−23.
(42) Knizia, G.; Adler, T.; Werner, H. Simplified CCSD(T)-F12 Methods: Theory and Benchmarks. *J. Chem. Phys.* **2009**, *130*, 054104.
(43) Purvis, G. D., III; Bartlett, R. J. A Full Coupled-Cluster Singles and Doubles Model: The Inclusion of Disconnected Triples. *J. Chem. Phys.* **1982**, *76*, 1910−18.
(44) Thomas, J.; DeLeeuw, B.; Vacek, G.; Schaefer, H., III A Systematic Theoretical Study of the Harmonic Vibrational Frequencies for Polyatomic Molecules - the Single, Double, and Perturbative Triple Excitation Coupled-Cluster (CCSD(T)) Method. *J. Chem. Phys.* **1993**, *98*, 1336−1344.
(45) Frisch, M. J.; Trucks, G. W.; Schlegel, H. B.; Scuseria, G. E.; Robb, M. A.; Cheeseman, J. R.; Scalmani, G.; Barone, V.; Mennucci, B.; Petersson, G. A.; et al. *Gaussian 09*; Gaussian: Wallingford, CT, 2009.
(46) Werner, H.-J.; Knowles, P. J.; Kinizia, G.; Manby, F. R.; Schutz, M.; Celani, P.; Korona, T.; Lindh, R. *Molpro*, Version 2010.1; Ab Initio Programs: Lexington, MA, 2010.
(47) Eyring, H.; Lin, S. H.; Lin, S. M. *Basic Chemical Kinetics*; Wiley: New York, 1980.
(48) Robinson, P. J.; Holbrook, K. A. *Unimolecular Reactions*; Prentice Hall: Engelwood Cliffs, NJ, 1972.
(49) Steinfield, J.; Francisco, J.; Hase, W. *Chemical Kinetics and Dynamics*; Englewood: Cliffs, NJ, 1989.
(50) Levine, R. D., Molecular Reaction Dynamics. *Molecular Reaction Dynamics*; Cambridge University Press: Cambridge, UK, 2005.